Estimation of lateral spreading by SPT, CPTU and DMT following the 2016 Mw7.8 Ecuador earthquake

S. Amoroso
Dept. of Engineering and Geology, University of Chieti-Pescara, Pescara, Italy, sara.amoroso@unich.it
Istituto Nazionale di Geofisica e Vulcanologia, L'Aquila Italy

K.M. Rollins
Dept. of Civil and Environmental Engineering, Brigham Young University, Provo, Utah, rollinsk@byu.edu

K. Wissmann
Geopier Foundation Company, Davidson, North Carolina, kwissmann@geopier.com

L. Minarelli
Istituto Nazionale di Geofisica e Vulcanologia, L'Aquila Italy, luca.minarelli@ingv.it

ABSTRACT: Earthquakes may induce liquefaction producing ground failures, including lateral spreading. Different approaches are proposed to estimate lateral spreading displacements, that account for the complex liquefaction-induced deformation patterns. Following the 2016 Mw7.8 Ecuador earthquake, several sites experienced liquefaction and lateral spreading due to the extreme ground motions and the presence of loose saturated silty sand deposits. This paper presents the in situ test data obtained at the Briceño Bridge embankment, where the foundation materials were reinforced by rammed aggregate piers preventing liquefaction-induced failures. Potential lateral displacements at the ground surface were computed using standard penetration test (SPT), piezocone test (CPTu) and flat dilatometer test (DMT) in natural and treated soils, and then compared with real observations. The results provide reasonable agreement between estimation and measurement, supporting the calibration of DMT liquefaction-induced displacement predictions for which no case histories are available.

Keywords: lateral spreading; rammed aggregate piers; standard penetration test (SPT); piezocone test (CPTu); flat dilatometer test (DMT)

1. Introduction

Earthquakes and related phenomena, such as liquefaction, can impact any human being due to economic or social reasons. In this respect, it would be prudent to adopt proactive earthquake design measures to manage the risk and prevent slope failures, bridge and building foundation failures, and flotation of buried structures, as stated also in several building codes.

During an earthquake, the occurrence of liquefaction induced pore pressures and their post-seismic dissipation can generate liquefaction-induced ground failures that distress man-made structures (e.g. [1], [2]). Generally, liquefaction-induced ground failures are divided into vertical displacements (ground settlement, ground slumps and structural settlement) and horizontal displacements (flow failure, lateral spread and ground oscillation). Lateral spread has been the most damaging consequence of liquefaction during recent earthquakes for gentle slopes or for nearly level (or gently inclined) ground with a free face (e.g. river banks, road cuts), as stated by Zhang et al. [3] and Youd [4].

The quantitative evaluation of liquefaction-induced lateral ground displacements is of extreme importance for engineering purposes. In this respect, different procedures for the deformation assessment have been developed using numerical modelling, laboratory tests, and in situ tests.

This paper focuses on a case study of the Briceño Bridge embankment, whose foundation materials were reinforced by Rammed Aggregate Pier® (RAP) elements preventing liquefaction-induced failures following the 2016 Mw7.8 Ecuador earthquake ([5], [6]). Potential lateral displacements at the ground surface were computed using methods based on the standard penetration test (SPT), piezocone test (CPTu) and flat dilatometer test (DMT) in natural and treated soils. The results predicted by different in situ tests, and the comparisons with real observations are presented, supporting also the calibration of a DMT liquefaction-induced displacement prediction method for which no case histories were previously available.

2. Estimation of lateral spreading using in-situ tests

Different methods using the standard penetration test (SPT) and cone penetration test (CPT) data have been developed for estimating lateral displacements resulting from liquefaction-induced lateral spread for horizontal or very gently sloping features (e.g. [7] [8] [9] [10], [4], [3]). These methods were mainly developed on the basis of case history data from previous earthquakes together with in situ and/or laboratory tests.

Zhang et al. [3] combined the available SPT- or CPT-based methods for predicting liquefaction factor of safety with laboratory cyclic shear strain testing to develop a procedure to estimate the potential maximum

cyclic shear strain for saturated sandy soils under seismic loading. Almost 300 liquefaction-induced lateral spreading observations associated with 12 past earthquakes were used to develop the lateral displacement index (*LDI*):

$$LDI = \int_0^{Z_{max}} \gamma_{max} dz \quad (1)$$

where γ_{max} = maximum cyclic shear strain estimated from relative density (D_r) and safety factor against liquefaction (*FSL*); Z_{max} = maximum depth below all the potential liquefiable layers with $FSL < 2.0$.

LDI was developed to quantify potential lateral displacements for a given soil profile, soil properties, and earthquake characteristics, without including geometric parameters characterizing ground geometry. Subsequently, Zhang et al. [3] correlated the lateral displacement (LD) for level ground with a free face with LDI using the equation:

$$LD = 6 \cdot LDI \cdot \left(\frac{L}{H}\right)^{-0.8} \quad (2)$$

where L = horizontal distance from the toe of the free face; H = free face height which is the elevation difference between the level ground surface and the toe of a free face.

Bartlett and Youd [9] initially developed a multiple linear regression (MLR) equation for lateral spread displacement using SPT data. Later, Youd et al. [10] updated the MLR procedure for predicting lateral displacement (D_H) using a database of more than 400 observations generated by 10 earthquakes to produce the equations:

$$\begin{aligned} \log D_H = & -16.713 + 1.532M - 1.406 \log R^* \\ & - 0.012R + 0.592 \log W + 0.540 \log T_{15} \\ & + 3.413 \log (100 - F_{15}) \\ & - 0.795 \log (D50_{15} + 0.1 \text{ mm}) \end{aligned} \quad (3)$$

$$R^* = R_0 + R \quad (4)$$

$$R_0 = 10^{(0.89 \cdot M - 5.64)} \quad (5)$$

where M = moment magnitude of the earthquake; R = horizontal distance from the site to the seismic energy source; T_{15} = cumulative thickness of saturated liquefiable granular layers with corrected blow counts $(N_1)_{60} < 15$; F_{15} = average fine content for granular material within the T_{15} layer; $D50_{15}$ = average mean size for granular material within the T_{15} layer; W = free face ratio, defined as the ratio between the height of the free face (H) and the horizontal distance (L) from the toe of the free face to the point in question.

Youd [4] extended the MLR procedure to CPT data by defining the boundary between contactive and dilative granular soils, by means of the state parameter (ψ). Granular soils with $(N_1)_{60} < 15$ are generally contractive and granular soils with $(N_1)_{60} > 15$ are generally dilative. Jefferies and Been [11] identified contractive behavior for $\psi \geq 0$, and dilative behavior for $\psi < 0$. According to Robertson and Cabal [12], the state parameter for uncemented, Holocene age, granular soils can be determined using only CPT data, by the equation:

$$\psi = 0.56 - 0.33 \log Q_{tn,cs} \quad (6)$$

where $Q_{tn,cs}$ = clean sand equivalent normalized cone resistance. For dune sands, Youd [4] suggested that $\psi < -0.08$ should be sufficiently dilative to prevent lateral spreading and recommended summing the thickness of layers with $\psi > -0.08$ to determine T_{15}.

However, the state parameter can also be estimated using the flat dilatometer test (DMT). Yu [13] presented a correlation equation for ψ based on the results of a finite element analysis of the DMT installation in four well-known reference sands modelled by the critical state model CASM ([14]):

$$\psi = 0.02 \cdot \left(\frac{K_D}{K_0}\right)^2 + 0.015 \cdot \left(\frac{K_D}{K_0}\right) + 0.026 \quad (7)$$

where K_D = horizontal stress index and K_0 = at-rest lateral stress coefficient.

The at-rest lateral stress coefficient is an important input in the evaluation of many geotechnical engineering problems and reliable direct measurement of in-situ K_0 in sands are often too expensive for most project budgets. Therefore, semi-empirical relationships based on common in-situ tests appear to be the most promising approach for accurately estimating K_0 in granular soils ([15]).

For example, Baldi et al. [16] developed a predictive relationship for K_0 based on DMT and CPT data from calibration chamber test results of two well-known reference sands:

$$K_0 = 0.376 + 0.095 K_D - 0.00172 \cdot \left(\frac{q_c}{\sigma_v'}\right) \quad (8)$$

where q_c = cone penetration resistance; σ_v' = effective vertical stress.

In addition, by considering the influence of the overconsolidation ratio (*OCR*) on K_0, Hossain and Andrus [15] developed a new correlation equation based on 26 sandy test sites:

$$\begin{aligned} K_0 = & \ 0.72 + 0.456 \log OCR + 0.035 K_D \\ & - 0.194 \log (q_c / \sigma_v') \end{aligned} \quad (9)$$

where *OCR* in sands can be estimated from DMT and CPT data according to Monaco et al. [17]:

$$\begin{aligned} OCR = & \ 0.0344(M/q_t)^2 - 0.4174 (M/q_t) \\ & + 2.2914 \end{aligned} \quad (10)$$

where M = constrained modulus and q_t = corrected cone penetration resistance.

3. Site characterization at Briceño Bridge Embankment

On April 16, 2016, a Mw7.8 earthquake occurred along the central Pacific coastline of Ecuador (Fig. 1a). The earthquake was located onshore, less than 10 km southeast of the city of Pedernales, with an hypocentral depth of 21 km, rupturing the central seismogenetic segment of the subduction interface zone between the Nazca and the continental plates ([18], Fig. 1a). Several site effects were surveyed from the day after the mainshock and for the following months by GEER-ACT [5] and Chunga et al. [18]. Particularly, liquefaction and its related effects were observed at numerous sites along the nortwest and west coast of Ecuador and many of these sites were studied and analyzed, some of them with various exploration techniques (e.g. shear wave velocity measurements,

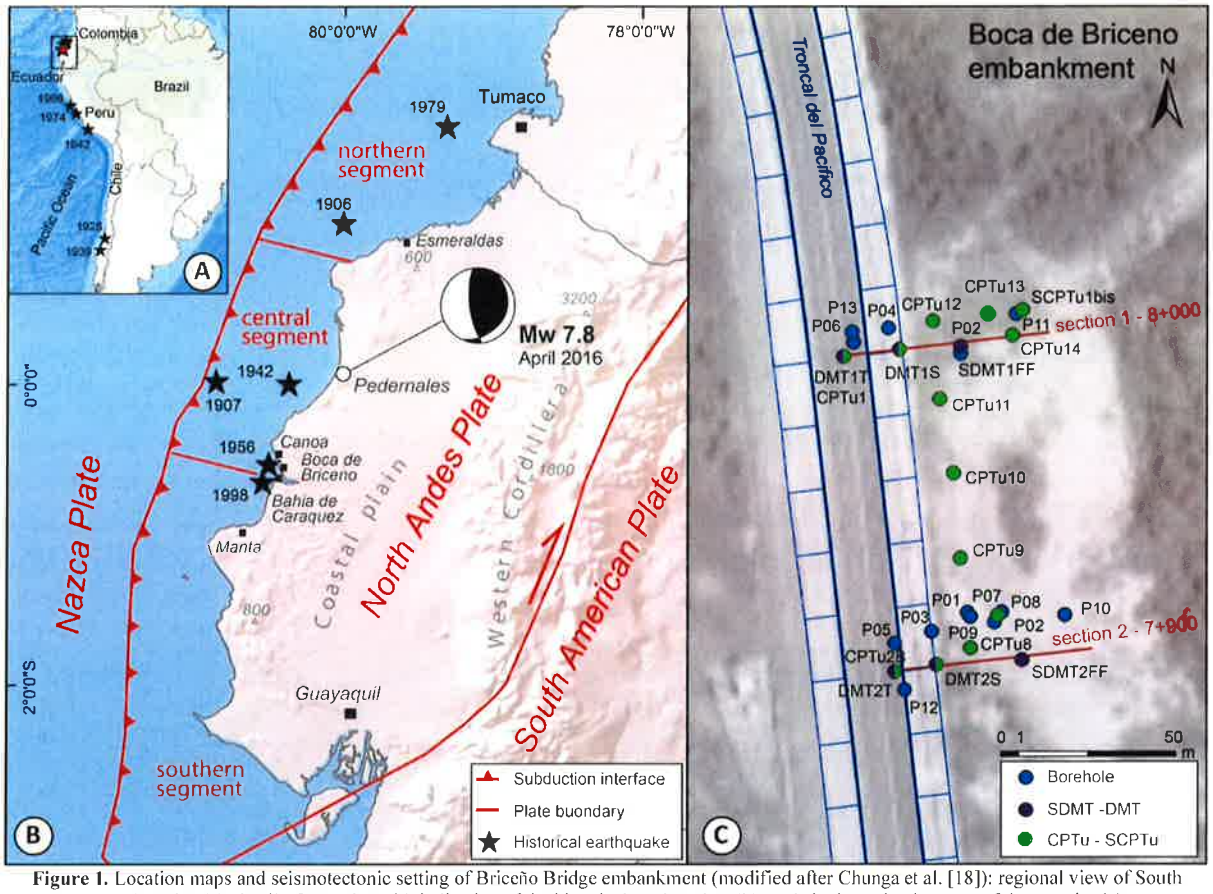

Figure 1. Location maps and seismotectonic setting of Briceño Bridge embankment (modified after Chunga et al. [18]): regional view of South America (a), detail of Ecuador with indication of the historical earthquakes (b); and site investigation map of the test site (c).

Chinese dynamic cone penetration tests, standard penetration tests, cone penetration tests and flat dilatometer tests), as reported by Vera-Grunauer et al. [19].

The Briceño Bridge embankment, part of the state road system, is located approximately 7 km from Canoa city (Fig. 1b). Undifferentiated alluvial terraces and deposits of the Recent Quaternary period characterize the area of Boca de Briceño. Those terraces and deposits involve the present hydrographic valley of the Rio Briceño, constituing the valley floor, and they consist of gravels, sands, silts and clays of extremely variable thickness.

The study area is about 112 km away from the 2016 epicenter (Fig. 1b). Due to earthquake directivity, the estimated peak ground acceleration (a_{max}) at the site was 0.4g ([20], [21]). During the GEER-Earthquake Recoinnassance, evidence of liquefaction was observed within meters of the embankment in the form of sand boils and sand ejecta through cracks in the ground adjacent to the bridge abutment. Neverthless, the embankment exhibited minimal damage (a repairable longitudinal crack of the pavement about 5-15 cm wide, with 1-3 cm of vertical displacement) while maintaining the serviceability of the road to the public ([5]). This behavior may be attributed to the rammed aggregate pier (RAP) ground improvement elements used to reinforce foundation materials preventing liquefaction-induced failures. Over 6000 RAPs were installed in 2012 beneath the 700 m-long Briceño Bridge embankment to mitigate liquefaction potential and to increase the global stability of the sand and silty sand deposits. The 0.51 m-diameter RAPs were installed to depths of about 5 m with spacings ranging from 1.65 m at the edges up to 3 m at the center of the embankment, corresponding to area replacement ratios of 9% and 3%, respectively ([6]).

RAP effectiveness has been well documented in clean sands following the 2010-2011 Canterbury Earthquake Sequence in New Zealand according to Wissmann et al. [22], Wentz et al. [23], Vautherin et al. [24], and Amoroso et al. [25], showing that densification can be obtained and reliably quantified by means of piezocone (CPTu) and flat dilatometer (DMT) measurements in granular soil deposits having a soil behaviour type index $I_c < 1.8$ or a material index $I_D > 1.8$, even at depths exceeding the design treatment depth. In contrast, only limited research is available to demonstrate RAP effectiveness in mitigating liquefaction in sandy silts and silty sands, based on recent blast-induced liquefaction testing following the 2012 Emilia-Romagna earthquake in Italy ([26]).

In this context, an extensive geotechnical site characterization campaign was performed mostly along two sections of the Briceño Bridge embankment, Section 1 and Section 2, in correspondance with two embankment cross-sections, Station km 8+000 and Station km 7+900, respectively (Fig. 1b), with the aim of examining in depth the mechanism involved in the liquefaction mitigation intervention and providing a better overall evaluation of mitigation effectiveness in the sandy and silty sand deposits. The site investigations

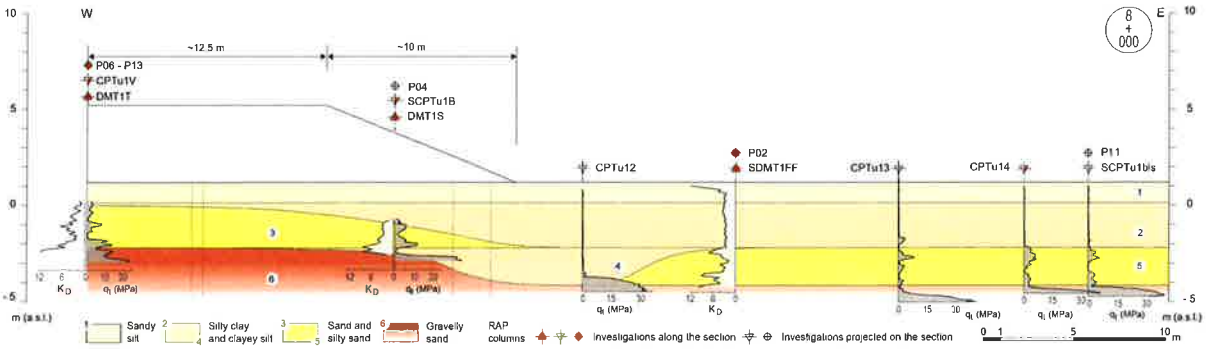

Figure 2. Section 1 – 8+000: geotechnical subsoil model by CPTU and DMT parameters.

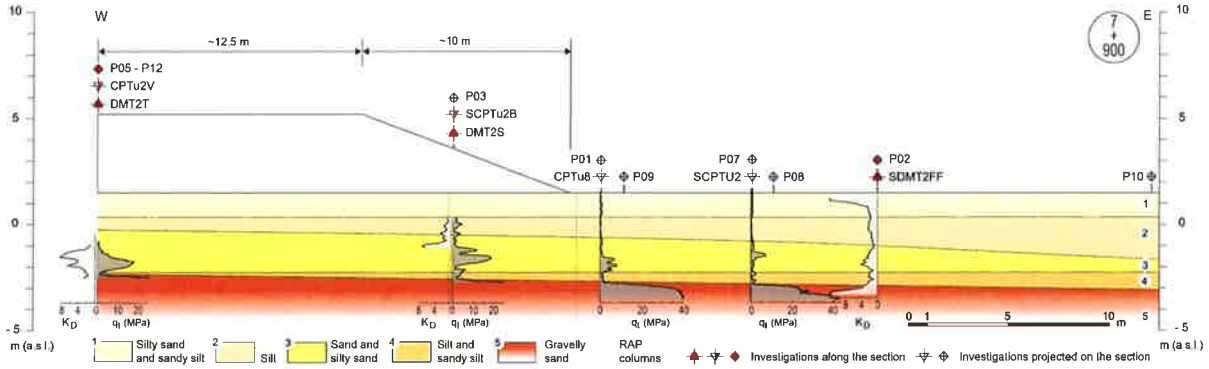

Figure 3. Section 2 – 7+900: geotechnical subsoil model by CPTU and DMT parameters.

consisted of: 13 boreholes along with along with standard penetration test (SPT) and disturbed soil sampling for grain size distribution analyses, determination of Atterberg limits and petrographic analyses; 16 piezocone tests (CPTu); 4 seismic piezocone tests (SCPTu); 5 flat dilatometet tests (DMT); 2 seismic dilatometer tests (SDMT); 10 dynamic penetration cross-hole tests (DPCH). Considering that the focus of the present study is related to the estimation of lateral spread by in situ tests, Fig. 1b shows the location of boreholes, CPTus, DMTs and SDMTs. Due to the presence to a bottom gravel layer, the depth of CPTu and DMT/SDMT tests was limited to 5-8 m, while boreholes were drilled up to 30 m.

At each section, at least one borehole, one CPTu and one DMT/SDMT were carried out on the top and on the slope of the embankment in the center of a pier group. In addition, similar tests were performed off the embankment, in free-field conditions, where liquefaction occurred after 2016 Ecuador earthquake. The DMT membrane was oriented such that it was inflated towards the piers, even though the orientation of the blade should do not have influenced the results, as shown by Marchetti et al. [27].

The subsoil characterization along the two sections was performed using the in situ geotechnical information. In particular, Section 1 (Fig. 2) and Section 2 (Fig. 3) were reconstructed using the material index (I_D) and horizontal stress index (K_D) profiles from DMT/SDMT tests, and the soil type behavior index (I_c) and corrected cone resistance (q_t) profiles from CPTu tests. The complex distribution of Boca de Briceño soil deposits reflects the depositional dynamics of the Rio Briceno channel and sea mouth. The sandy layers were deposited into the active fluvial channel, and, in the western portion, into the oceanic beach. Episodes of fluvial avulsion and creation of new river channels changed the active channel into low energy pond environments. Finer grained sediments, such as silts, silty clays and organic clays, accumulated into the abandonment ponds, developed into the former river channels. The changing depositional dynamics of the Briceño River therefore induced the rapid lateral variation in lithology between sands to silty sands (units 3 and 5 for Section 1 in Fig. 2; unit 3 for Section 2 in Fig. 3) and silts to clayey silts (units 2 and 4 for Section 1 in Fig. 2; unit 2 for Section 2 in Fig. 3), suggesting that the Briceño paleochannel has a curved path, not parallel to the bridge embankment.

Borehole logs together with SPT results and laboratory tests confirmed the high heterogeneity of the subsoil within the area of study. Fig. 4 summarizes this information in terms of corrected blow counts ($(N_1)_{60}$) and fines content (FC) for Section 1 and Section 2. Different colors were used to detect easily SPT and FC data on the top (blue) and on the slope (red) of the embankment, and in the free field (black).

According to a preliminary liquefaction assessment relative to the 2016 Pedernales earthquake ([6], [19]), the liquefied layer in the free field has a variable thickness between 1 and 3 m. This layer is composed of sands and silty sands (units 3 and 5 for Section 1 in Fig. 2; unit 3 for Section 2 in Fig. 3) and has a relevant fines content (FC) of approximately 15-20%. In contrast, the sand and silty sand deposits below the embankment were improved by RAP installation and were not susceptible to liquefaction, as indicated by their performance during the 2016 earthquake. The mechanism involved in the liquefaction mitigation is still under investigation, although Smith and

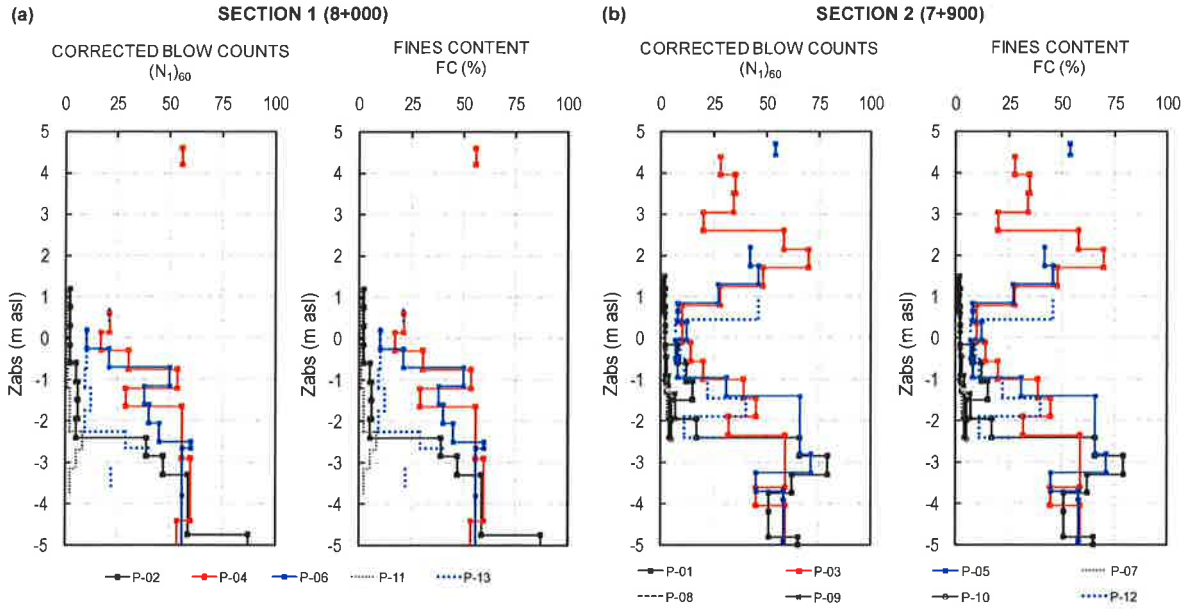

Figure 4. SPT results and FC profiles for Section 1 (a) and Section 2 (b). Different colors indicate different investigation locations: blue on the top and red on the slope of the embankment, and black in the free field.

Wissmann [6] preliminarly verified that pier installation densified the soil and increased the composite shear strength. In contrast, untreated silty sand deposits at sites such as the Meja Bridge embankment (167 km from the epicenter with a recorded a_{max} equal to 0.35g) experienced devasting effects from the earthquake due to the lateral displacement of the toe of the slope ([19]). Altogether, these observations motivated an investigation of the potential lateral displacements predicted using different in situ tests at the Briceño Bridge embankment in comparisons with real observations.

4. *Lateral spreading prediction following the Mw7.8 Ecuador earthquake*

The availability of CPTu, DMT and SPT tests, in natural and treated soil deposits, makes it possible to evaluate different approaches for estimating liquefaction-induced lateral displacements ([3], [10] [4]) for the case study of the Briceño Bridge embankment.

By considering the geometry of the two embankment segments, as reported in Figs. 2 and 3, the case study was analyzed as level ground with a free face. The well-established CPTu-based procedure proposed by Idriss and Boulanger [28] was used for the assessment of liquefaction susceptibility and therefore for the *FS* estimation, assuming the ground water table at 0.2 m a.s.l., M = 7.8 and a_{max} = 0.4g, while the D_r was evaluated from the correlation by Tatsuoka et al. [29]. Based on the liquefaction safety factor, the Zhang et al. [3] procedure was applied to the CPTu data under the top (CPTu1V, CPTu2V) and under the slope (SCPTu1B, SCPTu2B) of the embankment to evaluate the lateral displacement (*LD*), as summarized in Table 1.

LD values indicate slope movements of approximately of 0.5-0.8 m based on the CPTus at the top of the embankament, and of 1.2-1.6 m based on the CPTus on the slope of the embankment. These predictions do not fit well with the earthquake observations that refer to a maximum crack width of 5-15 cm. This aspect may be possibly explained by the higher variability of the Zhang et al. [3] method for *LD* < 1 m due to the small available dataset used to develop this approach at small lateral displacements. The overprediction may also be attributed to the extrapolation of lateral spread predictions to a thin layer composed of materials finer or more plastic than non-plastic silty sands ([4]).

Table 1. CPTu prediction by Zhang et al. (2004).

Location	CPTu	LDI (m)	L (m)	H (m)	LD (m)
Section 1 TOP	CPTu1V	0.55	22.50	4.00	0.83
Section 1 SLOPE	SCPTu1B	0.55	6.40	2.55	1.58
Section 2 TOP	CPTu2V	0.34	22.50	3.70	0.48
Section 2 SLOPE	SCPTu2B	0.44	5.60	2.10	1.20

Therefore, the Youd et al. [10] approach was also considered using the SPT data below the embankment. After correction, the blow counts were always greater than 15 within the sand and silty sand deposits identified by the borehole logs, as shown by the $(N_1)_{60}$ profiles on the top and on the slope of the embankment in Fig. 4. This implies that the predicted lateral displacement is equal to zero despite liquefaction within the saturated liquefiable granular layers because of the tendency for dilation during shear. This result fits well with the observed embankment performance during the 2016 earthquake. To estimate what lateral displacement would have occurred below the embankment without the piers, the Youd et al. [10] procedure was again applied below the embankment assuming that the untreated natural soil was the same as that analyzed in the free field along Section 1 and Section 2. In this respect, Table 2 summarizes the input data necessary to predict the lateral displacements (D_H). Potential liquefiable layers of at least approximately 1 m were

Table 2. SPT prediction by Youd et al. (2002).

Location	Borehole	Elevation (m asl)	$(N_1)_{60}$ (-)	T_{15} (m)	F_{15} (%)	$D50_{15}$ (mm)	H (m)	L (m)	W (%)	D_H (m)
Section 1 TOP	P-11	from -2.25 to -3.90	5.50	1.65	15.00	0.26	4.00	22.50	17.78	0.89
Section 1 SLOPE	P-11	from -2.25 to -3.90	5.50	1.65	15.00	0.26	2.55	6.40	39.84	1.09
Section 2 TOP	P-07	from -1.95 to -2.85	13.00	0.90	18.00	0.36	3.70	22.50	16.44	0.58
Section 2 TOP	P-08	from -1.95 to -2.85	5.50	0.90	17.50	0.22	3.70	22.50	16.44	0.67
Section 2 TOP	P-09	from -1.17 to -3.45	6.25	2.28	12.67	0.24	3.70	22.50	16.44	1.07
Section 2 TOP	P-10	from -2.00 to -3.35	4.33	1.35	19.50	0.17	3.70	22.50	16.44	0.82
Section 2 SLOPE	P-07	from -1.95 to -2.85	13.00	0.90	18.00	0.36	2.10	5.60	37.50	0.72
Section 2 SLOPE	P-08	from -1.95 to -2.85	5.50	0.90	17.50	0.22	2.10	5.60	37.50	0.83
Section 2 SLOPE	P-09	from -1.17 to -3.45	6.25	2.28	12.67	0.24	2.10	5.60	37.50	1.32
Section 2 SLOPE	P-10	from -2.00 to -3.35	4.33	1.35	19.50	0.17	2.10	5.60	37.50	1.01

Table 3. CPTu prediction by Youd (2018).

Location	CPTu	Elevation (m asl)	ψ (-)	T_{15} (m)	F_{15} (%)	$D50_{15}$ (mm)	H (m)	L (m)	W (%)	D_H (m)
Section 1 TOP	CPTu1V	from 0.2 to -1.78	-0.06	1.98	15.00	0.26	4.00	22.50	17.78	0.96
Section 1 SLOPE	SCPTu1B	from -0.70 to -1.78	-0.06	1.78	15.00	0.26	2.55	6.40	39.84	1.13
Section 2 TOP	CPTu2V	from -0.80 to -1.48	-0.01	0.90	18.00	0.36	3.70	22.50	16.44	0.58
Section 2 SLOPE	SCPTu2B	from -1.07 to -1.93	-0.11	0.86	18.00	0.36	2.10	5.60	37.50	0.0

Table 4. DMT prediction by Youd (2018).

Location	CPTu	Elevation (m asl)	K_0 (-)	ψ (-)	K_0 (-)	ψ (-)	T_{15} (m)	F_{15} (%)	$D50_{15}$ (mm)	H (m)	L (m)	W (%)	D_H (m)
			Baldi et al. (1986)		Hossain & Andrus (2016)								
Section 1 TOP	DMT1T	from -0.30 to -2.20	0.78	0.02	0.82	0.02	1.90	15.00	0.26	4.00	22.50	17.78	0.94
Section 1 SLOPE	DMT1S	from -1.40 to -2.50	0.78	0.01	0.82	0.02	1.10	15.00	0.26	2.55	6.40	39.84	0.91
Section 2 TOP	DMT2T	from -0.90 to -1.60	0.80	0.00	1.00	0.02	0.70	18.00	0.36	3.70	22.50	16.44	0.52
Section 2 SLOPE	DMT2S	from -0.40 to -1.10	0.80	0.01	1.00	0.02	0.70	18.00	0.36	2.10	5.60	37.50	0.65

considered with the aim of avoiding possible D_H overprediction ([4]). Based on SPT blow counts, the computed $D_H \approx 0.6$-1.1 m and $D_H \approx 0.7$-1.3 m on the top and of slope of the embankment, respectively, along both the sections. This implies that RAP installation mitigated liquefaction-induced lateral spreading during the 2016 Pedernales earthquake.

The MLR procedure was then extended to CPTu profiles on the top (CPTu1V, CPTu2V) and on the slope (SCPTu1B, SCPTu2B) of the embankement estimating the state parameter, as recently proposed by Youd [4]. With reference to the sandy and silty sandy units identified by I_c, Table 3 summarizes the information related to the CPTu predictions of the lateral displacements. CPTu results would suggest that failures under the embankment would have been equal to zero assuming a minimum threshold of $\psi < -0.01$, which is closer to 0 than the $\psi < -0.08$ threshold suggested by Youd [4].

However, in granular soil deposits ψ can also be evaluated using the DMT test ([14]) as noted previously. The availability of the earthquake observations and of the flat blade dilatometer measurements at Briceño Bridge embankment provide an interesting research opportunity for calibration of a DMT liquefaction-induced displacement prediction for which no case histories are available. With reference to the sandy and silty sand units identified by I_D, Table 4 shows the D_H predictions obtained from DMT profiles on the top (DMT1T, DMT2T) and on the slope (DMT1S, DMT2s) of the embankement along both the sections. In particular, ψ was derived by means of Eq. (7) that is a function of K_D and K_0. In this respect, Table 4 includes K_0 (and ψ therefore) values estimated by two different correlations that use coupled DMT-CPT parameters: Baldi et al. [16], as reported in Eq. (8), and Hossain and Andrus [15], as provided by Eq. (9). Both the K_0 methodologies agree and identify a clear threshold between contractive and dilative behavior at $\psi = 0.02$ for the sands and silty sands of the Briceño paleochannel. This limiting value includes also CPTu threshold and agrees with the considerations by Jefferies and Been [11], while it results farther from Youd [4] criteria for dune sands. However, the different value of the threshold may be related to the different geology (grain shape, mineralogy, grain size distribution and surface roughness of grains), in the different analyzed case histories, as also stated by Jeffreries and Been (2000).

Altogether the results provided by the different methods show that Youd et al. [10] approach, then updated by Youd [4], works better than Zhang et al. [3] at the Briceño Bridge embankment, since the MLR procedure predicted lateral displacements similar to the 2016 observations. In contrast Zhang et al. [3] method provides slope movements between 0.5 and 1.6 m that are not comparable with the earthquake evidences (maximum crack width of 5-15 cm).

5. Conclusions

Following the 2016 Mw7.8 Ecuador earthquake an extensive site campaign (boreholes, SPTs, CPTus/SCPTus, DMT/SDMTs, DPCHs, laboratory tests) was performed at the Briceño Bridge embankment, where the foundation materials were reinforced by rammed aggregate piers preventing liquefaction-induced failures. Flat dilatometer and piezocone tests allowed a detailed reconstruction of the subsoil model along two embankment sections. The complex distribution of Boca de Briceño soil deposits reflects the depositional dynamics of the Rio Briceno channel and coastline, suggesting that the Briceño paleochannel has a curved path, not parallel to the bridge embankment. This hetereogenity is clearly detected by I_D and K_D from DMT, by I_c and q_t from CPTu, and by SPT and laboratory information.

Potential lateral spread displacements at the ground surface computed at the test site using SPT and CPTu data in natural and treated soils, showed that the Zhang et al. [3] approach overestimates the embankment slope movements, while the Youd et al. [10] procedure provides lateral displacements in good agreement with the 2016 earthquake observations by considering potential liquefiable layers of at least approximately 1 m. This aspect may be possibly explained by the higher variability of Zhang et al. [3] method for $LD < 1$ m due to the small available dataset used to develop this approach at small lateral displacements. The overprediction may also be attributed to the extrapolation of lateral spread predictions to thin layers composed of materials finer or more plastic than non-plastic silty sands ([4]).

Finally the extension of the MLR procedure to the use of the state parameter ([4]) allowed, not only to predict lateral displacements by CPTu, but also by DMT. The availability of the earthquake observations and of the the flat blade dilatometer measurements at Briceño Bridge embankment provided an interesting research opportunity to evaluate the potential for a DMT-based lateral spread displacement prediction for which no case histories are available. The computed failures identify a clear threshold between contractive and dilative behavior at $\psi = 0.02$ for the sands and silty sands of the Briceño paleochannel, consistent with considerations by Jefferies and Been [11]. However, the different value of the threshold (if compared with Youd [4]) may be related to the different geology (grain shape, mineralogy, grain size distribution and surface roughness of grains), in the analyzed case histories, as also stated by Jeffreries and Been (2000).

Acknowledgement

A special thanks to "Studio Prof. Marchetti" (Rome, Italy) for kindly providing the SDMT apparatus to carry out the SDMT investigations in Ecuador, and to "Geoestudios" (Guayaquil, Ecuador) for gently assisting the proper performance of the site campaign.

References

[1] Hamada, M., O'Rourke, T. D. "Case studies of liquefaction and lifeline performance during past earthquakes", Volume 1, Japanese Case Studies, Technical Rep. NCEER-92-0001, National Center for Earthquake Engineering Research, Buffalo, N.Y, 1992.

[2] Kramer, S.L. "Geotechnical earthquake engineering", Prentice Hall, Upper Saddle River, N.J, 1996.

[3] Zhang, G., Robertson, P.K., Brachman, R.W.I. "Estimating liquefaction-induced lateral displacement using the standard penetration test of cone penetration test", J. Geotech. Geoenviron. Eng., 130(8), pp. 861–871, 2004.

[4] Youd, T.L. "Application of MLR procedure for prediction of liquefaction-induced lateral spread displacement", J. Geotech. Geoenviron. Eng., 144(6), 04018033, 2018.

[5] Geotechnical Extreme Events Reconnaissance Association–Applied Technology Council (GEER-ATC). "Earthquake Reconnaissance, Mw 7.8, April 16th, 2016, Muisne, Ecuador", Nikolaou, S., X. Vera-Grunauer, and R. Gilsanz (Editors), Version 1b, 604 pp., 2016. doi: 10.18118/G6F30N.

[6] Smith, M.E., Wissmann, K.. "Ground improvement reinforcement mechanisms determined for the Mw 7.8 Muisne, Ecuador, earthquake", In: 5th Geotechnical Earthquake Engineering and Soil Dynamics Conference: Liquefaction Triggering, Consequences, and Mitigation - GEESDV 2018, Austin, Texas, June 10-13, 2018, GSP 290, pp. 286-294.

[7] Rauch, A.F., Martin, J.R., II. "EPOLLS model for predicting average displacements on lateral spreads", J. Geotech. Geoenviron. Eng., 126(4), pp. 360–371, 2000.

[8] Bardet, J.P., Tobita,T., Mace, N., Hu, J. "Regional modeling of liquefaction-induced ground deformation", Earthquake Spectra, 18(1), pp. 19–46, 2002.

[9] Bartlett, S.F., Youd, T.L. "Empirical prediction of liquefaction-induced lateral spread", J. Geotech. Eng., 121(4), pp. 316–329, 1995.

[10] Youd, T.L., Hansen, C.M., Bartlett, S.F. "Revised multilinear regression equations for prediction of lateral spread displacement", J. Geotech. Geoenviron. Eng., 128(12), pp. 1007–1017, 2002.

[11] Jefferies, M., Been, K. "Soil liquefaction: A critical state approach", Taylor & Francis, New York, 2006.

[12] Robertson, P.K., Cabal, K.L., "Guide to Cone Penetration Testing for Geotechnical Engineering," 5th edition, Gregg Drilling & Testing, 131 pp., 2012.

[13] Yu, H.S. "In situ soil testing: from mechanics to interpretation", James K. Mitchell Lecture. In Geotechnical and Geophysical Site Characterization ISC'2, Porto, Portugal, Sept. 19-22, 2004, 36 pp.

[14] Yu, H.S. "CASM: A unified state parameter model for clay and sand", International Journal for Numerical and Analytical Methods in Geomechanics, 22, pp. 621-653, 1998.

[15] Hossain, M.A., Andrus, R.D., "At-rest lateral stress coefficient in sands from common field methods," J. Geotech. Geoenviron. Eng., 142(12), 06016016, 2016.

[16] Baldi, G., Bellotti R., Ghionna, V., Jamiolkowski, M., Marchetti, S., Pasqualini, E. "Flat Dilatometer Tests in Calibration Chambers", In: In Situ '86, ASCE Spec. Conf. on Use of In Situ Tests in Geotechn. Engineering, Virginia Tech, Blacksburg, VA, June, 1986, GSP 6, pp. 431-446.

[17] Monaco, P., Amoroso, S., Marchetti, S., Marchetti, D., Totani, G., Cola, S., Simonini, P., "Overconsolidation and stiffness of Venice Lagoon sands and silts from SDMT and CPTU", J. Geotech. Geoenviron. Eng., 140(1), pp. 215-227, 2014. https://doi.org/10.1061/(ASCE)GT.1943-5606.0000965

[18] Chunga, K., Livio, F., Mulas, M., Ochoa-Cornejo, F., Besenzon, D., Ferrario, M.F., Michetti, A.M. "Earthquake ground effects and intensity of the 16 April 2016 Mw 7.8 Pedernales, Ecuador, earthquake: implications for the source characterization of large subduction earthquakes", Bulletin of the Seismological Society of America, 108(6), pp. 3384-3397, 2018.

[19] Vera-Grunauer, X.F., Lopez-Zhindon, S., Ordonez-Rendon, J., Chavez-Abril, M.A. "Liquefaction case histories after the 2016 megathrust Pedemales earthquake in Ecuador", In: 7th International Conference on Eartquake Geotechnical Engineering – 7 ICEGE, Rome, Italy, June, 17-20, 2019, pp. 805-820.

[20] Ye, L., Kanamori, H., Avouac, J.P., Li, L., Cheung, K.F., Lay, T. "The 16 April 2016, Mw 7.8 (Ms 7.5) Ecuador earthquake: a quasirepeat of the 1942 Ms 7.5 earthquake and partial re-rupture

of the 1906 Ms 8.6 Colombia–Ecuador earthquake", Earth Planet. Sci. Lett. 454, pp. 248–258, 2016.
[21] Beauval, C., Marinière, J., Laurendeau, A., Singaucho, J.C., Viracucha, C., Vallée, M., Maufroy, E., Mercerat, D., Yepes, H., Ruiz, M., Alvarado, A. "Comparison of observed ground motion attenuation for the 16 April 2016 Mw 7.8 Ecuador megathrust earthquake and its two largest aftershocks with existing ground motion prediction equations", Seismol. Res. Lett. 88(2A), pp. 287–299, 2017.
[22] Wissmann, K.J., van Ballegooy, S., Metcalfe, B.C., Dismuke, J.N., Anderson, C.K. "Rammed aggregate pier ground improvement as liquefaction method in sandy and silty soils", In: 6th International Conference on Earthquake Geotechnical Engineering - 6ICEGE, Christchurch, New Zealand, Nov., 2-4, 2015.
[23] Wentz, F.J., van Ballegooy, S., Rollins, K.M., Ashford, S.A., Olsen, M.J. "Large Scale Testing of Shallow Ground Improvements using Blast-Induced Liquefaction", In: 6th International Conference on Earthquake Geotechnical Engineering - 6ICEGE, Christchurch, New Zealand, Nov., 2-4, 2015.
[24] Vautherin, E., Lambert, C., Barry-Macaulay, D., Smith, M. "Performance of rammed aggregate piers as a soil densification method in sandy and silty soils: experience from the Christchurch rebuild", In: 3rd International Conference on Performance-based Design in Earthquake Geotechnical Engineering - PBD-III, Vancouver, Canada, July, 16-19, 2017.
[25] Amoroso, S., Rollins, K.M., Monaco, P., Holtrigter, M., Thorp, A. Monitoring ground improvement using the seismic dilatometer in Christchurch, New Zealand. Geotechnical Testing Journal 41(5), pp. 946-966, 2018. https://doi.org/10.1520/GTJ20170376
[26] Amoroso, S., Rollins, K.M., Andersen, P., Gottardi, G., Tonni, L., García Martínez, M.F., Wissmann, K., Minarelli, L. "Full-scale testing of liquefaction mitigation using rammed aggregate piers in silty sands", In: 7th International Conference on Eartquake Geotechnical Engineering – 7 ICEGE, Rome, Italy, June 17-20, 2019, 656-663.
[27] Marchetti, S., Totani, G., Taddei B., Monaco, P. "Indagini di anisotropia tensionale per la diagnosi della stabilità dei pendii", Attività di Ricerca nell'anno 1986-87, Gruppo Nazionale per il Coordinamento per gli studi di Ingegneria Geotecnica del Consiglio Nazionale delle Ricerchem Comitato Nazionale per le Scienze di Ingegneria e Architettura, October 1987 (in Italian).
[28] Idriss, I.M., Boulanger, R.W. "Soil liquefaction during earthquakes", Earthquake Engineering Research Institute, MNO.12, Oakland, CA, 2008.
[29] Tatsuoka, F., Zhou, S., Sato, T., Shibuya, S. "Method of evaluating liquefaction potential and its application", Report on Seismic hazards in the soil deposits in urban areas, Ministry of Education of Japan, pp.75–109, 1990 (in Japanese).